AIAA JOURNAL
Vol. 48, No. 8, August 2010

Component Modal Tests with Additional Mass and Stiffness

Masayoshi Misawa*
Shizuoka University, Hamamatsu 432-8561, Japan

DOI: 10.2514/1.J050304

This paper describes a method to predict the dynamic characteristics of large structures, such as satellite antennas and solar paddles. It has become increasingly difficult to perform modal tests for large space structures, because they are not strong enough to withstand the force of gravity. Component modal tests are effective at identifying the dynamic characteristics of structures consisting of several components. In this method, the effect of untested components are considered as additional mass and stiffness attached to a tested component. Additional mass and stiffness, attached to an arbitrary coordinate, are found by reducing mass and stiffness matrices of untested components. Modal tests for different tested components give identical frequencies, so these frequencies are considered the frequencies of structures. The feature of the proposed method is to obtain the dynamic characteristics of large structures with component modal tests and to need no component mode synthesis. Numerical examples show that the proposed method has the potential to predict the dynamic characteristics of large structures by component modal tests.

Nomenclature

f_{exact}	=	structure frequency calculated by finite-element analysis without modeling errors, Hz
f_{test}	=	measured frequency in simulated component modal tests, Hz
$\boldsymbol{K}$	=	stiffness matrix
$\bar{K}$	=	reduced stiffness
$\boldsymbol{M}$	=	mass matrix
$\bar{M}$	=	reduced mass
$\boldsymbol{R}$	=	transformation vector
$\boldsymbol{x}$	=	displacement vector
ΔK	=	additional stiffness
ΔM	=	additional mass
σ	=	frequency used in finding additional mass and stiffness, Hz
ω	=	angular frequency, rad/s

Subscripts

p	=	translational coordinate with additional mass and stiffness
q	=	coordinates without additional mass and stiffness
s	=	quantity of structures
t	=	quantity of tested components

I. Introduction

LARGE satellite antennas are one of the key technologies needed to realize high-quality economical satellite communication systems. There are problems to overcome in developing large satellite antennas. The dynamic characteristics of space structures play an important role in the design of control systems. It is required to confirm the dynamic characteristics of antennas by modal tests, even though antennas have increased in size. However, large flexible structures cause the full-scale ground tests to be impossible sometimes, because they are not strong enough to withstand the force of gravity. The focus of the research into this problem is to confirm the dynamic characteristics of large structures without testing the whole structure.

Component mode synthesis (CMS) is an effective method to find the dynamic characteristics of large structures consisting of several components. Various methods have been proposed and are grouped into several types according to the component modes used to represent the components. All the methods provide the coupled equation of motion by imposing compatibility relations on the boundary coordinates obtained in each component. By selecting component modes, the order of the eigenvalue solution is reduced. In the mid-1960s, Hurty reported an analytical approach to CMS [1]. Craig and Bampton simplified Hurty's method [2]. They formulated CMS using fixed-interface normal modes with a set of constraint modes. A method to find accurate interface modes using dynamic reduction was presented for improving the accuracy of frequency prediction in which the boundary coordinates are modal coordinates in the reduced equation of motion [3]. However, it is difficult to fix the boundaries of components in actual modal tests. The use of free–free normal modes eliminates the need for constraint modes, but this results in solutions that are more susceptible to truncation error in higher modes. MacNeal [4] and Rubin [5] introduced a set of shape functions, termed residual modes, to minimize the truncation error. Benfield and Hruda [6] improved the accuracy by applying two types of external loading to the free boundary coordinates of the component under consideration. The component is loaded at its boundary with mass and stiffness contributions from the remaining components. Kammer and Baker [7] made a theoretical and numerical comparison between the fixed-interface Craig–Bampton method [2] and the free-interface method of MacNeal and Rubin [4] for component substructure representation. Qui et al. introduced a method using mixed modes [8]. There were different approaches dealing with the relative dynamic importance of constraint modes to create accurate reduced-order models [9,10]. An overview of CMS can be found in [11].

The relationship of component analysis to component testing was investigated for test verification of finite-element models. For use in test-analysis correlation, test-analysis models were developed using the new reduction formulation for component finite-element models to predict exact frequencies and modes of structures [12]. Martinez et al. used free–free modes and the residual flexibility at the boundary of the tested component to create a test-analysis model of the entire structure [13]. Constrained modes and frequencies were derived using free boundary modes and residual flexibility for large complex structures to verify constrained models [14]. Baker [15] pointed out that the use of residual flexibility with free–free modes is the only method that is experimentally feasible.

Presented as Paper 2006-1660 at the 47th AIAA/ASME/ASCE/AHS/ASC Structures, Structural Dynamics, and Materials Conference, Newport, RI, 1–4 May 2006; received 20 October 2009; revision received 03 February 2010; accepted for publication 14 March 2010.

*Professor, Department of Mechanical Engineering, 3-5-1 Johoku, Naka-ku. Senior Member AIAA.

In experimental approaches, an experimental CMS procedure was presented [16]. This procedure uses identification of individual components and assembles a global model of the coupled structural dynamics through equivalent mass and stiffness representations of the components. Morgan et al. presented an experimentally-based method of CMS to predict the forced response of structure [17]. This method uses test-derived CMS matrices and the uncoupled forced response of each substructure. The forced response of structure is predicted by considering the internal coupling forces and external applied forces on a substructure independently and superimposing the responses of each.

New approaches (the mass-additive method) were presented. Admire et al. used the mass-additive method in a modal test to avoid problems associated with design and development of test fixtures for space shuttle payloads [18]. Karpel and Raveh [19] and Karpel and Ricci [20] proposed a method to test components with boundary coordinates loaded with rigid, heavy dummy masses supported by soft springs. Dummy masses generate local displacements near the boundaries to predict the dynamic properties of the entire structures. The method was applied to a space-type structure to demonstrate the effectiveness of the component modal test [21]. Chandler and Tinker proposed a method for coupling substructures using mass-additive mode. This method is an approach in which known masses are attached to the boundaries of the test article to exercise the interfaces and bring the interface modes into the frequency range of the global modes [22]. This paper has shown that the mass-additive mode synthesis technique including constraint modes worked well. Soucy and Humar [23] proposed an approach to CMS in which the characteristics of individual components are determined experimentally through modal and static tests. Komatsu et al. [24] improved the predicted dynamic characteristics of structures with rotational displacements found by introducing a polynomial approximation for the measured modes. These methods need CMS to obtain the dynamic characteristics of structures. Misawa and Funamoto [25] proposed a method to predict the dynamic characteristics of large structures with component modal tests. In this method, to simulate the dynamic behavior of structures, reduced mass and stiffness matrices of untested components are replaced with a mass and a spring attached to a tested component. The feature of this method is to predict natural frequencies and modes of large structures with component modal tests and needs no CMS.

This paper describes a method to determine a coordinate with additional mass and stiffness in component modal tests. In this method, the effect of untested components is considered as additional mass and stiffness attached to a tested component. At first, this paper describes how to find additional mass and stiffness. Next, a procedure to select a mass and stiffness additive coordinate and a tested component subjected to modal tests is shown. Finally, numerical examples are given to demonstrate the effectiveness of the method.

II. Formulation

In general, finite-element models of complex structures have modeling errors. However, it is assumed that there are no modeling errors, because the main purpose of this paper is to confirm whether the proposed method has the potential to predict natural frequencies and modes of structures. The author hopes to address the effect of modeling errors in future works to apply the proposed method to real structures [26].

A. Additional Mass and Stiffness

Consider large structures consisting of several elastic components interconnected, as shown in Fig. 1, and select a tested component subjected to modal tests. A tested component includes one or more components. The rest of the components are untested components. In Fig. 1, component 4 is the tested component, and components 1, 2, and 3 are untested. As the modal test of a tested component never gives the dynamic characteristics of structures, the effect of untested components is considered as additional mass and stiffness. In this study, additional mass and stiffness are attached to a translational coordinate on a tested component and they are attached to the same

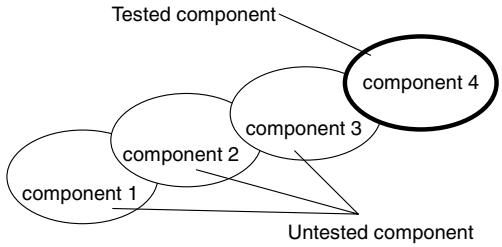

Fig. 1 Large structure consisting of several components.

coordinate. Figure 2 shows a test configuration with additional mass and stiffness at a translational coordinate on a tested component. After the completion of the modal test, a different tested component is selected. In this way, modal tests are performed for different tested components. Identical frequencies obtained by component modal tests are considered as frequencies of structures.

Denoting a translational coordinate with additional mass and stiffness as p and the rest as q, the dynamic equation of structures is expressed as

$$\omega_s^2 \begin{bmatrix} \boldsymbol{M}_{s,qq} & \boldsymbol{M}_{s,qp} \\ \boldsymbol{M}_{s,pq} & M_{s,pp} \end{bmatrix} \begin{Bmatrix} \boldsymbol{x}_{s,q} \\ x_{s,p} \end{Bmatrix} = \begin{bmatrix} \boldsymbol{K}_{s,qq} & \boldsymbol{K}_{s,qp} \\ \boldsymbol{K}_{s,pq} & K_{s,pp} \end{bmatrix} \begin{Bmatrix} \boldsymbol{x}_{s,q} \\ x_{s,p} \end{Bmatrix} \tag{1}$$

The following displacement relation is obtained from the first equation of Eq. (1):

$$\boldsymbol{x}_{s,q} = x_{s,p} \boldsymbol{R}_s \tag{2}$$

where

$$\boldsymbol{R}_s = -[\boldsymbol{K}_{s,qq} - (2\pi\sigma_s)^2 \boldsymbol{M}_{s,qq}]^{-1} [\boldsymbol{K}_{s,qp} - (2\pi\sigma_s)^2 \boldsymbol{M}_{s,qp}] \tag{3}$$

Note that displacement $x_{s,p}$ is scalar, because the number for coordinate p is one in this study. In addition, note that frequency σ_s is not a natural frequency of the structure but an arbitrary frequency used in mass and stiffness matrices reduction. To address this, σ_s is used in place of the frequency of structure f_s in Eq. (3). The dynamic equation of structures is reduced to coordinate p, using Eq. (2) as

$$-\omega_s^2 \bar{M}_s x_{s,p} + \bar{K}_s x_{s,p} = 0 \tag{4}$$

where

$$\bar{M}_s = \begin{Bmatrix} \boldsymbol{R}_s \\ 1 \end{Bmatrix}^T \boldsymbol{M}_s \begin{Bmatrix} \boldsymbol{R}_s \\ 1 \end{Bmatrix}; \qquad \bar{K}_s = \begin{Bmatrix} \boldsymbol{R}_s \\ 1 \end{Bmatrix}^T \boldsymbol{K}_s \begin{Bmatrix} \boldsymbol{R}_s \\ 1 \end{Bmatrix} \tag{5}$$

Equation (5) shows that distributed mass $\boldsymbol{M}_s$ of structures is replaced with a lumped mass (reduced mass $\bar{M}_s$) attached to a coordinate p. In a similar way, the displacement relation is obtained from the dynamic equation of the tested component as

$$\boldsymbol{x}_{t,q} = x_{t,p} \boldsymbol{R}_t \tag{6}$$

By reducing the dynamic equation of the tested component to the same coordinate p, the following equation is obtained:

$$-\omega_t^2 \bar{M}_t x_{t,p} + \bar{K}_t x_{t,p} = 0 \tag{7}$$

where

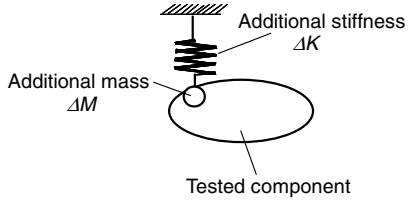

Fig. 2 Test configuration.

$$\bar{M}_t = \begin{Bmatrix} \boldsymbol{R}_t \\ 1 \end{Bmatrix}^T \boldsymbol{M}_t \begin{Bmatrix} \boldsymbol{R}_t \\ 1 \end{Bmatrix}; \qquad \bar{K}_t = \begin{Bmatrix} \boldsymbol{R}_t \\ 1 \end{Bmatrix}^T \boldsymbol{K}_t \begin{Bmatrix} \boldsymbol{R}_t \\ 1 \end{Bmatrix} \tag{8}$$

Distributed mass $\boldsymbol{M}_t$ of tested components is also replaced with a lumped mass (reduced mass $\bar{M}_t$) attached to the same coordinate p. Reduced mass $\bar{M}_s$ and stiffness $\bar{K}_s$ include the effect of untested components, but reduced mass $\bar{M}_t$ and stiffness $\bar{K}_t$ do not include it. Therefore, the difference between $\bar{M}_s$ and $\bar{M}_t$ ($\bar{K}_s$ and $\bar{K}_t$) denotes the effect of untested components, and additional mass and additional stiffness are expressed by

$$\left.\begin{aligned} \Delta M &= \bar{M}_s - \bar{M}_t \\ \Delta K &= \bar{K}_s - \bar{K}_t \end{aligned}\right\} \tag{9}$$

By adding additional mass and stiffness to a translational coordinate p, the dynamic equation of the tested component is obtained as

$$-\omega^2 \tilde{\boldsymbol{M}} \tilde{\boldsymbol{x}} + \tilde{\boldsymbol{K}} \tilde{\boldsymbol{x}} = \boldsymbol{0} \tag{10}$$

where

$$\left.\begin{aligned} \tilde{\boldsymbol{M}} &= \begin{bmatrix} \boldsymbol{M}_{t,qq} & \boldsymbol{M}_{t,qp} \\ \boldsymbol{M}_{t,pq} & M_{t,pp} + \Delta M \end{bmatrix} \\ \tilde{\boldsymbol{K}} &= \begin{bmatrix} \boldsymbol{K}_{t,qq} & \boldsymbol{K}_{t,qp} \\ \boldsymbol{K}_{t,pq} & K_{t,pp} + \Delta K \end{bmatrix} \end{aligned}\right\} \tag{11}$$

Equation (10) is considered the dynamic equation of structures, because the effect of untested components is taken into account as additional mass and stiffness. Although matrices $\tilde{\boldsymbol{M}}$ and $\tilde{\boldsymbol{K}}$ vary with a mass-additive coordinate and a tested component, the solutions of Eq. (10) give the frequencies and modes of the structure by selecting a mass-additive coordinate and a tested component appropriately. Namely, it is possible to measure the frequencies and modes of structures through component modal tests with additional mass and stiffness.

B. Mass and Stiffness Additive Coordinate

A coordinate with additional mass and stiffness has a significant effect on measuring accurate frequencies of structures. Because additional mass and stiffness are attached to the same coordinate in this study, this paper shows only how to select a mass-additive coordinate in the following. Masses ΔM, $\bar{M}_s$, and $\bar{M}_t$ are calculated with transformation vectors $\boldsymbol{R}$. Therefore, variations in these masses depend on transformation vectors. Considering reduced mass $\bar{M}_s$ as an example, the following equation is obtained by rewriting Eq. (3):

$$[\boldsymbol{K}_{s,qq} - (2\pi\sigma_s)^2 \boldsymbol{M}_{s,qq}]\boldsymbol{x}_{s,q} = -x_{s,p}[\boldsymbol{K}_{s,qp} - (2\pi\sigma_s)^2 \boldsymbol{M}_{s,qp}] \tag{12}$$

When frequency σ_s increases from zero, there are frequencies where $[\boldsymbol{K}_{s,qp} - (2\pi\sigma_s)^2 \boldsymbol{M}_{s,qp}]$ nearly becomes the null vector. Even if displacement $x_{s.p}$ is not zero, the right-hand side of Eq. (12) is considered to approximately equal zero, as

$$[\boldsymbol{K}_{s,qq} - (2\pi\sigma_s)^2 \boldsymbol{M}_{s,qq}]\boldsymbol{x}_{s.q} = \boldsymbol{0} \tag{13}$$

Frequencies satisfying Eq. (13) are equal to the natural frequencies of the structure with a mass-additive coordinate fixed. Because additional mass is attached to a fixed coordinate, reduced mass $\bar{M}_s$ calculated with these frequencies is large enough to generate displacement at the coordinate (these frequencies are called peak frequencies). If a node of the target mode of the structure is selected as a mass-additive coordinate, the peak frequency is identical to the target frequency of the structure. Therefore, when one of the peak frequencies of $\bar{M}_s$ approaches the target frequency of the structure, an extremely large additional mass is required to measure the target frequency in component modal tests, which may cause a serious problem that requires us to consider the strength of the tested component. In addition, variation in additional mass becomes large near the target frequency, even if the variation in frequency σ_s is small. For this reason, it is difficult to obtain accurate frequency of the structure by component modal tests. The best way to avoid these problems is to separate the peak frequency of $\bar{M}_s$ from the target frequency. Namely, for accurate frequency measurement with small additional mass in component modal tests, it is effective to select a mass-additive coordinate with large displacement of the target mode. Therefore, first a proposed coordinate with large displacement of the target mode is selected for a mass-additive coordinate.

In a similar way, reduced mass $\bar{M}_t$ also has peak frequencies that are equal to the natural frequencies of the tested component with a mass-additive coordinate fixed. Because masses $\bar{M}_s$ and $\bar{M}_t$ vary with frequency σ and have peaks at different frequencies, there exist frequency ranges where $\bar{M}_t$ is greater than $\bar{M}_s$. Therefore, additional mass ΔM has a negative value near the peak frequencies of $\bar{M}_t$. When one of the peak frequencies approaches the target frequency of the structure, it is impossible to measure the target frequency by component modal tests because of negative additional mass. To obtain a positive additional mass, a mass-additive coordinate is selected so that peak frequencies can be separated from the target frequency of the structure. It is required to confirm that additional mass is positive near the target frequency for the proposed coordinate selected, as mentioned previously. If additional mass has a positive value, the proposed coordinate is selected as a mass-additive coordinate. If this is not the case, it is required to reconfirm whether additional mass is positive or negative near the target frequency for other proposed coordinates with the next largest displacement. The procedure is repeated to select a mass-additive coordinate until the additional mass is positive.

Reduced stiffnesses $\bar{K}_s$ and $\bar{K}_t$ are calculated with the transformation vectors used in calculating $\bar{M}_s$ and $\bar{M}_t$. Therefore, the stiffness additive coordinate is the same as the mass-additive coordinate.

C. Selection of Tested Components

It is important which component is selected as a tested component for the measurement of the target mode. When unsuitable tested components are selected, it is difficult to obtain an accurate target mode, even if mass and stiffness additive coordinates are selected as mentioned previously. Consider the second mode of a cantilever beam, shown in Fig. 3 as an example. Because the boundary location of a tested component is free, displacement at the boundary is seldom small in component modal tests, even though mass and stiffness are attached to the optimal location. A large mass should be added at the boundary to obtain the second mode with small boundary displacement. This means that it is impossible to obtain the target mode by procedure to select mass-additive coordinates when the boundary of the tested component is close to the node of the target mode. Therefore, it is needed to select a tested component so that the boundary is separated from nodes of the target mode to measure accurate target modes of the structures with light additional mass. Because there is quite a possibility that a proposed coordinate changes for different tested components, a mass-additive location is selected anew.

III. Numerical Examples

Numerical results are given to demonstrate the effectiveness of the proposed method. Because component modal tests are not performed, the simulated test models are constructed by using finite-element models of tested components with additional mass and additional

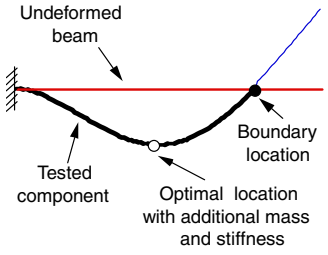

Fig. 3 Second mode of a cantilever beam.

stiffness. Natural frequencies and modes obtained by solving Eq. (10) are considered to be measured frequencies and modes in component modal tests.

A. Cantilever Beam

Consider a cantilever beam, made of CFRP (carbon fiber reinforced plastics), consisting of two components, as shown in Fig. 4. Arabic numbers show the location number. The boundary location is location 9. Each element length is 100 mm. Figure 4 also shows the test configuration of tested components with additional mass ΔM and additional stiffness ΔK. The subscripts of ΔM and ΔK show a tested component number. For example, in testing component 1, ΔM_1 and ΔK_1 are attached to component 1, considering the effects of component 2. Additional stiffness is created by a wire (and spring if required) suspending the tested component. For simplicity, only bending modes in the X–Y plane are considered. Therefore, additional mass and stiffness are attached to the Y coordinate of a location on the tested component. In this case, a tested component is set so that the Y axis is parallel to the gravitational force when performing component modal tests.

Table 1 shows analytical beam frequencies. These frequencies are used to confirm that the proposed method is effective to obtain frequencies of structures by simulated component tests.

1. *Variation in Additional Mass and Stiffness*

Figure 5 shows an example of mass variations with frequency σ used in calculating reduced masses. The tested component is component 1, and additional mass and stiffness are attached to boundary location 9. As reduced masses $\bar{M}_t$ and $\bar{M}_s$ are obtained by reducing mass matrices of the tested component and the beam, it is reasonable to suggest that $\bar{M}_s$ is greater than $\bar{M}_t$. However, it can be seen in Fig. 5 that there exists a frequency range where $\bar{M}_t$ is greater than $\bar{M}_s$, because $\bar{M}_t$ increases at its peak frequencies. Additional mass takes negative values near the peak frequency (20 to 24 Hz) of $\bar{M}_t$. Discontinuity in additional mass variation in Fig. 5 shows the frequency range where additional mass is negative. From the definition of additional mass, shown in Eq. (9), additional mass ΔM_1 has the same peak frequencies as mass $\bar{M}_s$. Because $\bar{M}_t$ is very small at the peak frequencies of $\bar{M}_s$, variations in ΔM_1 and $\bar{M}_s$ are almost identical. This is always true even if any component is selected as the tested component.

Figure 6 indicates variations in additional mass and stiffness when they are attached to boundary location 9. Because additional mass and stiffness are calculated with the same transformation vector $\boldsymbol{R}$, variations in ΔM_1 and ΔK_1 (ΔM_2 and ΔK_2) have the same tendency, though they have a different value. Namely, additional mass and stiffness have the same peak frequencies and frequency ranges with negative additional mass and stiffness. It also can be seen in Fig. 6 that additional masses ΔM_1 and ΔM_2 (additional stiffnesses ΔK_1 and ΔK_2) have almost the same variations. Considering additional mass as an example, this is why variation in additional mass does not depend on $\bar{M}_t$ but $\bar{M}_s$, because additional mass is almost determined by $\bar{M}_s$. The only difference in mass variation is the frequency range where additional mass has negative values, because the peak frequency of $\bar{M}_t$ varies with a tested component selected in each component modal test. These results are not peculiar in the case of adding additional mass to the boundary location. As additional stiffness has the same variation as additional mass, only the results concerning additional mass are shown in the following section. The description on the case in which component 1 is the tested component is given because of space limitation.

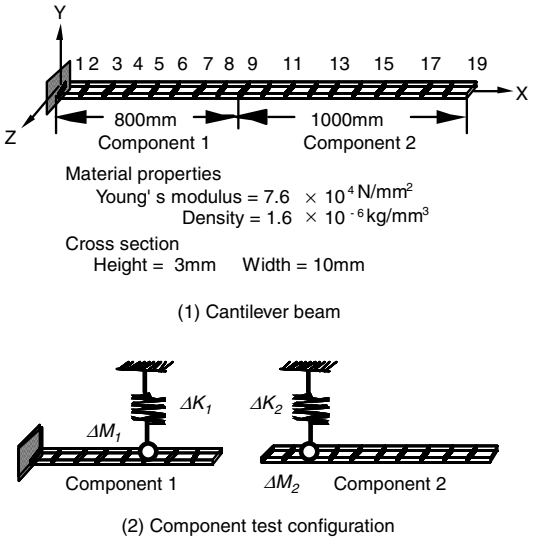

Fig. 4 Test configuration.

Table 1 Analytical natural frequencies of the beam

Mode number	Frequency, Hz
1	1.0
2	6.4
3	17.9
4	35.0
5	57.9

2. *Mass and Stiffness Additive Coordinate*

Figure 7 shows variations in the peak frequency of $\bar{M}_s$ when additional mass and stiffness are attached to each location of the beam. The first peak frequency increases from the first beam frequency $f_{s,1}$ and almost equals the second beam frequency $f_{s,2}$ for location 15. As stated in Sec. II.B, peak frequencies of $\bar{M}_s$ are equal to the natural frequencies of the structure with a mass-additive coordinate fixed. Because location 15 is the node of the second mode, the first peak frequency of $\bar{M}_s$ equals the second beam frequency $f_{s,2}$. The second peak frequency equals the third beam frequency $f_{s,3}$ for locations 10 and 17, and the peak frequency is separated from beam frequencies for location 14, where the peak frequency has a minimal value. Locations 10 and 17 are the node, and location 14 is the loop of the third beam mode. This implies that it is effective to select a

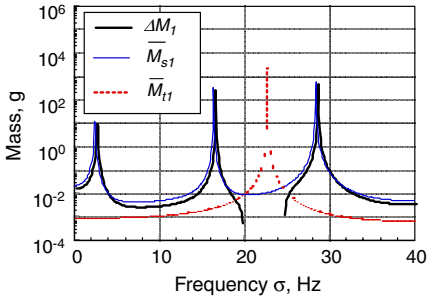

Fig. 5 Mass variations.

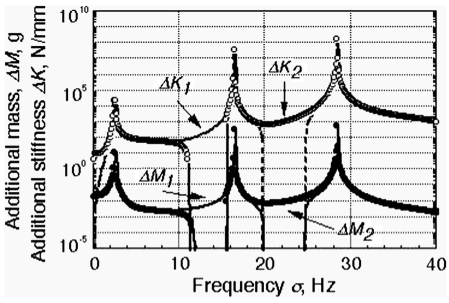

Fig. 6 Variations in additional mass and stiffness.

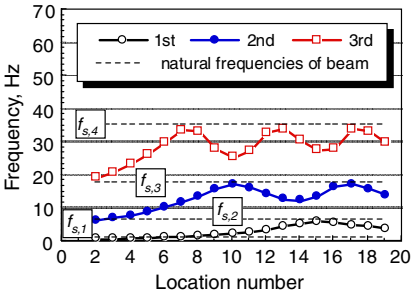

Fig. 7 Variations in peak frequencies of reduced mass $\bar{M}_s$.

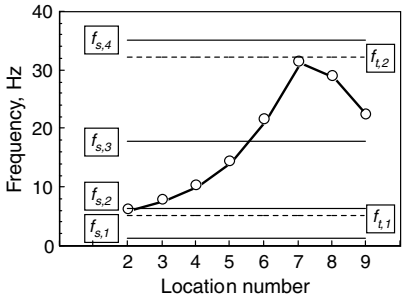

Fig. 8 Variations in peak frequencies of reduced mass $\bar{M}_t$.

location with large displacement for separating peak frequencies from the target frequency of the beam. Table 2 lists proposed coordinates with additional mass and stiffness on the tested component (component 1). In this table, $9Y$ shows coordinate Y at location 9.

Figure 8 shows variations in the peak frequency of $\bar{M}_t$ when additional mass and stiffness are attached to each location of the tested component (component 1). The peak frequencies are equal to natural frequencies of tested components with their mass-additive coordinate fixed. To avoid negative additional mass and stiffness, a coordinate is selected so that peak frequencies of $\bar{M}_t$ are kept away from target frequencies of the beam. The proposed coordinate is $9Y$ for the first frequency measurement. It can be seen in Fig. 8 that the peak frequency for location 9 is separated from the first frequency $f_{s,1}$ of the beam. Therefore, coordinate $9Y$ is a mass-additive coordinate having a positive additional mass. When the target frequency is of the second frequency, the proposed coordinate is $9Y$. Because the peak frequency for location 9 is separated from the second frequency $f_{s,2}$ of the beam, coordinate $9Y$ is selected as a mass-additive coordinate.

For the measurement of the third frequency $f_{s,3}$, Fig. 8 shows that the peak frequency for location 6 is close to the third frequency $f_{s,3}$ of the beam. This suggests that the proposed coordinate $6Y$ may not be appropriate for a mass-additive coordinate because of negative additional mass. For this reason, the author checked whether the additional mass is positive or negative. Figure 9 shows variations in reduced masses $\bar{M}_s$ and $\bar{M}_t$ for mass-additive coordinates $6Y$ and $7Y$. For the proposed coordinate $6Y$, the peak frequency of $\bar{M}_t$ is located near the third frequency $f_{s,3}$ of the beam, and the additional mass is negative near the target frequency, because $\bar{M}_t$ is greater than $\bar{M}_s$. Therefore, proposed coordinate $6Y$ is not selected as the mass-additive coordinate. Another mass-additive coordinate must be found, so it is able to confirm whether the additional mass is positive for the next proposed coordinate $7Y$. Figure 9 shows that the peak frequency of $\bar{M}_t$ is separated from the target frequency, and that the additional mass is positive. Coordinate $7Y$ should be selected for the third frequency measurement. However, the third mode cannot be obtained in this case, because it is difficult to keep boundary displacement small by adding additional mass to coordinate $7Y$, as described in Sec. III.A.3. In case the boundary of a tested component is close to the node of the target mode, another tested component should be selected.

In the same way, coordinates $5Y$ and $8Y$ for the fourth and fifth frequency measurements are mass-additive coordinates, respectively.

Table 2 Proposed coordinates in testing component 1

Mode number	Modal amplitude	
	Largest	Next
1	$9Y$	$8Y$
2	$9Y$	$8Y$
3	$6Y$	$7Y$
4	$5Y$	$4Y$
5	$8Y$	$4Y$

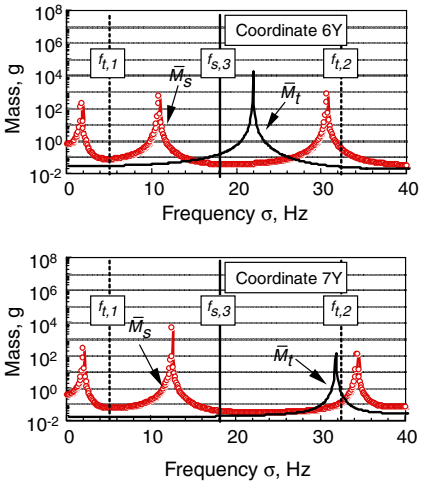

Fig. 9 Variations in reduced masses for mass-additive locations 6 and 7.

3. *Simulated Test Results*

Since frequency σ can take arbitrary values to find additional mass and stiffness, additional mass and stiffness vary with σ. When frequency σ equals the natural frequency of structure, the displacement relationship shown in Eq. (2) always holds, and the dynamic behavior of structure is simulated. However, there is not any information about the height of the natural frequencies of structure, because the author deals with large structures that are difficult to perform modal tests on the ground. Therefore, it is necessary to confirm the effect of frequency σ on the measured frequencies and modes in component modal tests. Variation in frequency accuracy is checked based on the location of additional mass and stiffness. Figure 10 shows the accuracy of the first frequency with the σ error used in calculation of additional mass and stiffness. A beam frequency calculated by finite-element analysis without modeling errors is f_{exact}, and f_{test} is a simulated test frequency of component 1 with boundary location 9. The simulated test frequencies are the solutions of Eq. (10). It should be noted that zero in the σ error means no error in finite-element models and has a natural frequency identical to the exact frequency of the beam. The frequency accuracy is high, as the displacement of mass-additive coordinates is large. The accuracy of the first frequency is more than 95%, regardless of the mass-additive coordinate. When the mass-additive coordinate is $9Y$, the first beam frequency can be obtained for the σ error of $\pm 10\%$. In other words, additional mass and stiffness variations are very small with σ. Therefore, it is possible to accurately measure the frequency of the target frequency, even if the analytical frequency of the structure including modeling error is used as frequency σ.

The similarity between exact and simulated test modes is checked using the modal assurance criteria (MAC). The results are listed in Table 3. For the first mode, MAC is almost one, and the simulated test mode is identical to the exact mode.

Figure 11 shows the accuracy of the second frequency. It can be seen in Fig. 11 that the accuracy of the second frequency is more than

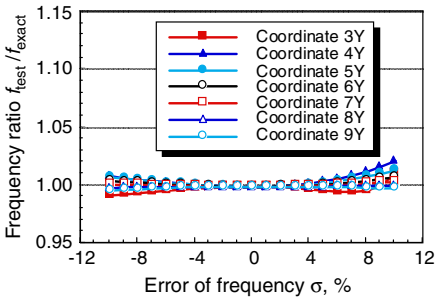

Fig. 10 Accuracy of the first frequency (boundary is location 9).

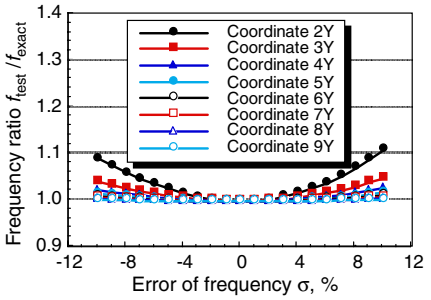

Fig. 11 Accuracy of the second frequency (boundary is location 9).

95%, except for coordinate 2Y. The second beam frequency can be obtained by selecting coordinate 9Y as the mass-additive coordinate. Also, in this case, there is the possibility to measure the accurate mode, because MAC is 0.99, as shown in Table 3.

On the other hand, tested component has a great influence on the accuracy of the third frequency and mode. Figure 12 shows the third frequency accuracy. Frequency accuracy is the highest when coordinate 7Y is a mass-additive coordinate. However, MAC shows that the simulated test mode is different from the exact mode for the third mode, as shown in Table 3. This suggests that it is difficult to obtain the third mode of the beam, though the third frequency is obtained with component modal tests. The author checked the third mode obtained from simulated component modal tests. Figure 13 shows the third mode of the beam and simulated test modes for different mass-additive coordinates. When the boundary is location 9, the simulated test mode is significantly different from the target mode. Because boundary location 9 is close to the node of the third mode, it is difficult to obtain small boundary displacement by attaching additional mass to coordinate 7Y. The only way to obtain the third mode with small boundary displacement is to add a large mass at the boundary (coordinate 9Y), as shown in Fig. 13. However, the author deals with large structures that are difficult to measure frequencies. Namely, frequency σ has an error. The accuracy of the third frequency decreases by 30% for the σ error of 10%, as shown in Fig. 12. This means that it is not necessarily effective for obtaining the accurate third frequency and mode of the beam, even if mass is attached to boundary coordinate 9Y. In this case, a tested component should be selected to separate the boundary location from the node of a target mode. Figure 14 shows the accuracy of the third frequency for different boundary locations and tested components. Frequency accuracy is improved by selecting location 12 as the boundary of tested component. Frequency accuracy is more than 95% for the σ error of $\pm$10%, so it is possible to accurately measure the third frequency, even if analytical frequency of the beam including modeling error is used as frequency σ. Because almost identical frequency is obtained by different tested components, this frequency is considered to be the third frequency of the beam. MAC increases by selecting location 12 as the boundary location for the third mode measurement. In the same way, MAC of the fifth mode also increases, as shown in Table 3. Therefore, the target mode of the beam can be obtained by selecting a tested component so that the boundary location is separated from the node of target mode.

Table 4 shows selected coordinates with additional mass and stiffness for different boundary locations. Coordinates listed in the second column show mass-additive coordinates that frequency and mode accuracy are the highest for each boundary location. Coordinates selected by the proposed method are identical to the

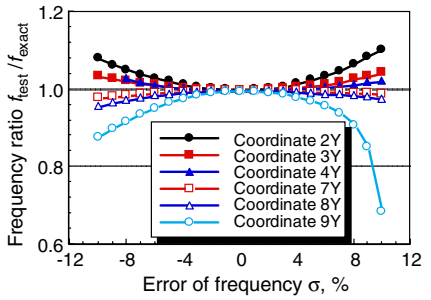

Fig. 12 Accuracy of the third frequency (boundary is location 9).

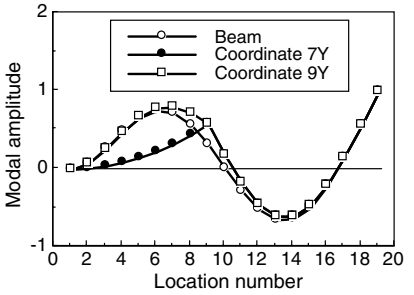

Fig. 13 Third mode for different mass-additive coordinates.

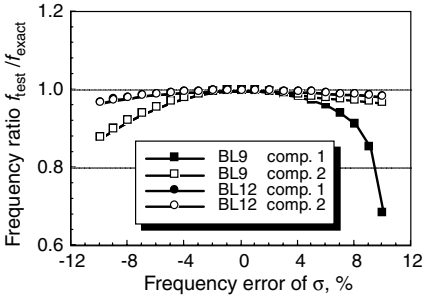

Fig. 14 Accuracy of the third frequency for boundary locations 9 and 12. (BL denotes boundary location.)

Table 3 MAC of exact and simulated test modes

Mode number	Boundary location 9	Boundary location 12
1	1.00	——
2	0.99	——
3	0.79	0.94
4	0.95	——
5	0.78	0.91

Table 4 Selected coordinates for tested component 1

Mode number	Frequency and mode accuracy	Proposed method	Boundary location
1	9Y	9Y	9
2	9Y	9Y	9
3	7Y	7Y	12
4	5Y	5Y	9
5	12Y	12Y	12

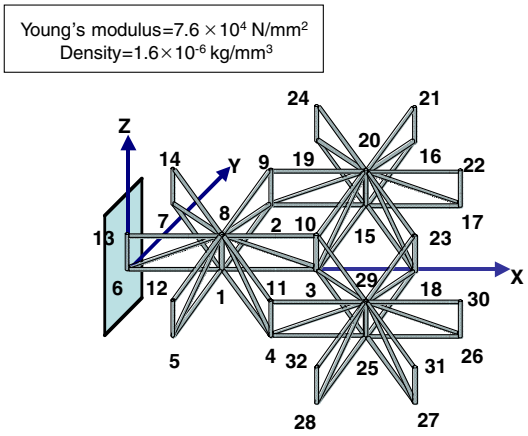

(1) Analytical model

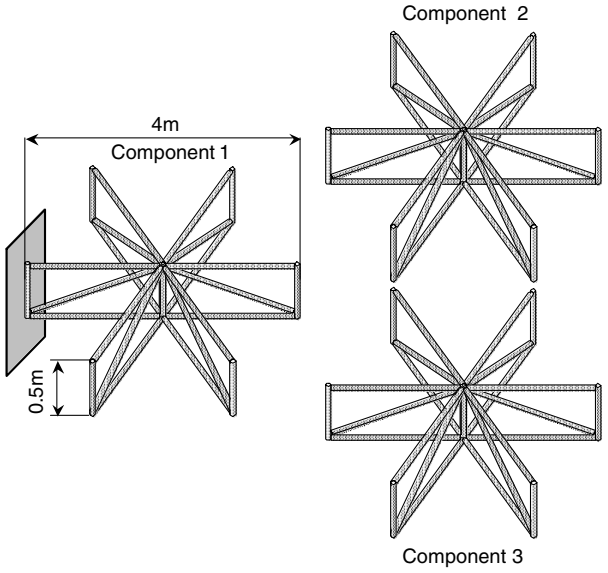

(2) Components

Fig. 15 Truss structure consisting of three components.

ones giving the highest frequency and mode accuracy. Therefore, the proposed method may have the potential to determine a coordinate with additional mass and stiffness and a tested component for accurate frequency and mode measurements of large structures in component modal tests.

B. Truss Structure

As an example of complicated structures, a truss structure is selected to demonstrate the effectiveness of the proposed method. This structure is a backup structure of deployable mesh antenna for satellite use [27]. Figure 15 shows a truss structure consisting of three components that have identical configuration and the same material properties. The total number of locations is 32. Locations 6 and 13 are interfaced with the satellite and are fixed in the dynamic analysis of the truss structure.

A proposed coordinate is a coordinate with a large displacement of the truss structure. The lower three modes of the truss structure are the first bending mode in the Y direction, the torsional mode about the X axis, and the second bending mode in the Y direction, respectively. For example, the proposed coordinate is $10Y$ for the first and second frequency measurements and $9Y$ for the third frequency measurement in testing component 1.

To obtain a positive additional mass, a mass-additive coordinate is selected so that peak frequencies of $\bar{M}_t$ can be separated from target frequencies of the structure. These frequencies are found by finite-element analysis. It is confirmed that additional mass is positive near

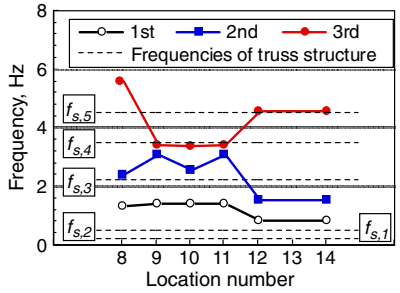

Fig. 16 Variation in peak frequency of reduced mass $\bar{M}_t$.

the target frequency for the proposed coordinate selected. Figure 16 shows variation in the peak frequency of $\bar{M}_t$ when the tested component is component 1. The first peak frequency is not close to the target frequency $f_{s,1}$ for the first frequency measurement when the proposed coordinate is $10Y$. Therefore, the proposed coordinate $10Y$ is selected as a mass-additive coordinate. For the second frequency measurement, the peak frequency for the proposed coordinate $10Y$ is separated from the target frequency $f_{s,2}$. Therefore, proposed coordinate $10Y$ is a mass-additive coordinate. In a similar way, a coordinate with additional mass and stiffness is selected for each frequency measurement for every different tested component. Table 5 lists the selected coordinates.

Simulated test frequencies of a tested component are calculated when additional mass and stiffness are attached to the selected coordinate, shown in Table 5. Table 6 shows calculated frequencies. For the first frequency measurement, frequencies of 0.21, 1.50, and 2.65 Hz are obtained when component 1 is the tested component. Additional mass and stiffness are calculated with the analytical first frequency of the truss structure as frequency σ. When component 2 is the tested component, the frequencies of 0.0, 0.21, and 5.69 Hz are obtained. The identical frequency obtained by component modal tests is considered the first frequency of the truss structure. The bold numbers in Table 6 show the predicted natural frequency of the truss structure. The predicted frequencies of the truss structure agree with the analytical frequencies of the structure. This means that component modal tests using different tested components can provide target frequencies. Therefore, the proposed method has the

Table 5 Selected coordinates for truss structure

Tested component	1st freq.	2nd freq.	3rd freq.
Component 1	10	10	9
Component 2	20	20	20
Component 3	29	29	29
Components 1 and 2	10	12	8
Components 1 and 3	10	12	8
Components 2 and 3	22	22	30

Table 6 Frequencies in simulated tests

Tested component no.	Mode no.	Target frequency, Hz: 1st freq.	2nd freq.	3rd freq.
1	1	**0.21**	**0.47**	1.48
	2	1.50	1.49	**2.18**
	3	2.65	2.63	3.28
2	1	0.00	0.00	0.00
	2	**0.21**	**0.47**	**2.18**
	3	5.69	5.69	5.69
1 and 2	1	**0.21**	0.29	0.48
	2	0.58	**0.47**	0.68
	3	1.86	0.61	**2.18**
2 and 3	1	**0.21**	**0.47**	0.81
	2	1.50	1.50	1.50
	3	2.39	2.37	**2.18**

potential to give useful information to determine which frequency corresponds to the frequency of the truss structure.

IV. Conclusions

The method using an efficient component modal test is described for obtaining the dynamic characteristics of large structures consisting of several components. The untested components considered are additional mass and stiffness so that the tested component behaves as a part of vibrating structures. Simulated component modal test results significantly depend on a location with additional mass and stiffness and a tested component subjected to modal test. In the proposed method, peak frequencies of two reduced masses give key information to select a location from a point of frequency accuracy. These masses are found by reducing mass matrices of a tested component and a structure to an arbitrary degree of freedom. This method selects the location so that peak frequencies of two masses are separated from a target frequency of structure to measure accurate frequency of structures in component modal tests. For mode accuracy, the target mode of structures is obtained by selecting a tested component whose boundary is separated from nodes of the target mode. Numerical examples show that the proposed method is effective and that results identical to exact solutions (frequencies and modes of structures) are obtained. The proposed method has the potential to be applicable in complex structures.

References

[1] Hurty, W. C., "Dynamic Analysis of Structural Systems by Component Modes," *AIAA Journal*, Vol. 3, No. 4, 1965, pp. 678–685. doi:10.2514/3.2947

[2] Craig, R. R., Jr., and Bampton, M. C. C., "Coupling of Substructures for Dynamic Analyses," *AIAA Journal*, Vol. 6, No. 7, 1968, pp. 1313–1319. doi:10.2514/3.4741

[3] Misawa, M., and Katayama, H., "Improvement of Boundary Modes in Component Mode Synthesis," 21st International Modal Analysis Conference, Society for Experimental Mechanics Paper 13, 2003.

[4] MacNeal, R. H., "A Hybrid Method of Component Mode Synthesis," *Computers and Structures*, Vol. 1, No. 4, 1971, pp. 581–601. doi:10.1016/0045-7949(71)90031-9

[5] Rubin, S., "Improved Component-Mode Representation for Structural Dynamic Analysis," *AIAA Journal*, Vol. 13, No. 8, 1975, pp. 995–1006. doi:10.2514/3.60497

[6] Benfield, W. A., and Hruda, R. F., "Vibration Analysis of Structures by Component Mode Substitution," *AIAA Journal*, Vol. 9, No. 7, 1971, pp. 1255–1261. doi:10.2514/3.49936

[7] Kammer, D. C., and Baker, M., "Comparison of the Craig–Bampton and Residual Flexibility Methods of Substructure Representation," *Journal of Aircraft*, Vol. 24, No. 4, 1987, pp. 262–267. doi:10.2514/3.45435

[8] Qui, J., Ying, Z., and Yam, L. H., "New Modal Synthesis Technique Using Mixed Modes," *AIAA Journal*, Vol. 35, No. 12, 1997, pp. 1869–1875. doi:10.2514/2.46

[9] Kammer, D. C., and Triller, M. J., "Selection of Component Modes for Craig–Bampton Substructure Representations," *Journal of Vibration and Acoustics*, Vol. 118, No. 2, 1996, pp. 264–270. doi:10.1115/1.2889657

[10] Simon, D. M., and Cost, T. L., "Selection of Characteristic Constraint Modes of Component Mode Synthesis Using a Modification of Effective Interface Mass," 46th AIAA/ASME/ASCE/AHS/ASC Structures, Structural Dynamics and Materials Conference, AIAA Paper 2005-2343, 2005.

[11] Craig, R. R., Jr., "Coupling of Substructures for Dynamic Analyses: an Overview," 41st AIAA/ASME/ASCE/AHS/ASC Structures, Structural Dynamics and Materials Conference, AIAA Paper 2000-1573, 2000.

[12] Kammer, D. C., and Flanigan, C. C., "Development of Test-Analysis Models for Large Space Structures Using Substructure Representations," *Journal of Spacecraft and Rockets*, Vol. 28, No. 2, 1991, pp. 244–250. doi:10.2514/3.26237

[13] Martinez, D. R., Carne, T. G., Gregory, D. L., and Miller, A. K., "Combined Experimental/Analytical Modeling Using Component Mode Synthesis," 25th AIAA/ASME/ASCE/AHS Structures, Structural Dynamics and Materials Conference, AIAA Paper 1984-0941, 1984.

[14] Admire, J. R., Tinker, M. L., and Ivey, E. W., "Residual Flexibility Test Method for Verification of Constrained Structural Modes," *AIAA Journal*, Vol. 32, No. 1, 1994, pp. 170–183. doi:10.2514/3.11963

[15] Baker, M., "Component Mode Synthesis Methods for Test-Based, Rigidly Connected Flexible Components," *Journal of Spacecraft and Rockets*, Vol. 23, No. 3, 1986, pp. 316–322. doi:10.2514/3.25114

[16] Alvin, K. F., Peterson, L. D., and Park, K. C., "Minimal-Order Experimental Component Mode Synthesis: New Results and Challenges," *AIAA Journal*, Vol. 33, No. 8, 1995, pp. 1477–1485. doi:10.2514/3.12570

[17] Morgan, J. A., Pierre, C., and Hulbert, G. M., "Forced Response of Coupled Substructures Using Experimentally Based Component Mode Synthesis," *AIAA Journal*, Vol. 35, No. 2, 1997, pp. 334–339. doi:10.2514/2.97

[18] Admire, J. R., Tinker, M. L., and Ivey, E. W., "Mass-Additive Modal Test Method for Verification of Constrained Structural Models," *AIAA Journal*, Vol. 31, No. 11, 1993, pp. 2148–2153. doi:10.2514/3.11903

[19] Karpel, M., and Raveh, D., "Fictitious Mass Element in Structural Dynamics," *AIAA Journal*, Vol. 34, No. 3, 1996, pp. 607–613. doi:10.2514/3.13111

[20] Karpel, M., and Ricci, S., "Experimental Modal Analysis of Large Structures by Substructuring," *Mechanical Systems and Signal Processing*, Vol. 11, No. 2, 1997, pp. 245–256. doi:10.1006/mssp.1996.0076

[21] Karpel, M., Raveh, D., and Ricci, S., "Ground Modal Tests of Space-Structure Component Using Boundary Masses," *Journal of Spacecraft and Rockets*, Vol. 33, No. 2, 1996, pp. 272–277. doi:10.2514/3.26752

[22] Chandler, K. O., and Tinker, M. L., "A General Mass-Additive Method for Component Mode Synthesis," 38th AIAA/ASME/ASCE/AHS/ASC Structures, Structural Dynamics, and Materials Conference, AIAA Paper 1997-1381, 1997.

[23] Soucy, Y., and Humar, J. L., "Experimental Verification of a Test-Based Hybrid Component Mode Synthesis Approach," *AIAA Journal*, Vol. 41, No. 5, 2003, pp. 912–923. doi:10.2514/2.2027

[24] Komatsu, K., Sano, M., Kai, T., Tsujihata, A., and Mitsuma, H., "Experimental Modal Analysis for Dynamic Models of Spacecraft," *Journal of Guidance, Control, and Dynamics*, Vol. 14, No. 3, 1991, pp. 686–688. doi:10.2514/3.20696

[25] Misawa, M., and Funamoto, K., "Dynamic Characteristic Prediction of Large Satellite Antennas by Component Tests," *Journal of Spacecraft and Rockets*, Vol. 42, No. 5, 2005, pp. 845–849. doi:10.2514/1.10503

[26] Misawa, M., and Kawasoe, H., "Component Modal Tests to Identify the Dynamic Characteristics of Large Structures: Effect of Modeling Errors," SEM Annual Conference and Exposition on Experimental and Applied Mechanics, Society for Experimental Mechanics Paper 34, 2009.

[27] Mitsugi, J., Yasaka, T., and Miura, K., "Shape Control of the Tension Truss Antenna," *AIAA Journal*, Vol. 28, No. 2, 1990, pp. 316–322. doi:10.2514/3.10391

J. Wei
Associate Editor